INTERNATIONAL JOURNAL FOR ENGINEERING ANALYSIS AND DESIGN, VOL. 1, 189-214 (1994)

ANALYSIS OF LAMINATED COMPOSITE PLATES WITH THREE-DIMENSIONAL LAYER-WISE CONSTANT SHEAR ELEMENTS

EVER J. BARBERO[1] and RAFFAELE ZINNO[2]

[1] *Dept. of Mech. & Aer. Engng., West Virginia University, Morgantown, WV, USA*

[2] *Dept. of Struct. Engng., University of Calabria, Cosenza, Italy*

ABSTRACT

A new three-dimensional element with two-dimensional kinematic constraints is used for the linear analysis of laminated composite plates. The element can represent plates with variable number of layers and thickness, including ply drop-off problems. The element is validated by the "*Patch test*" for the case of isotropic and laminated plates. In particular a refined computation of stresses is performed by integrating the equilibrium equations through an assembly of elements that represents the laminate. Some examples are reported to show the capability of the element to predict the mechanical behaviour of this kind of structures. An interface with the NISA commercial program is developed and used for the pre- and post-processing of the results.

1. INTRODUCTION

Multilayered composites are appropriate structural materials in weight sensitive aerospace applications where high strength-to-weight ratios are needed. A large body of technical literature has been published on the subject. Much of the analysis tools were originally developed for thin plates, based on Kirchhoff-Love kinematic assumptions. As it is well known, the classical laminate theory underpredicts the deformation energy because transverse shear strains are neglected. In fact as the plate becomes thicker compared to its in-plane dimensions, the transverse effects become more pronounced, especially in the case of laminated composite plates because of their low transverse shear moduli compared to their longitudinal moduli.

Reissner studied these effects on elastic plates [1] and on sandwich type shells [2], while Mindlin included rotatory inertia terms in the dynamic analysis of plates [3]. Reddy [4] applied the First Shear Deformation Theory (FSDT) for the analysis of laminated composite plates and shells. The FSDT produces excellent results (e.g. deflections, fundamental vibration frequencies, etc.) but the accuracy of the stress distribution does not improve significantly over the Kirchhoff-Love Theory (Classical Plate Theory - CPT) and is not satisfactory. The determination of the stresses is very important for the solution of crucial aspects in the optimal design of composite laminates, like the determination of the ultimate load carrying capacity obtained by the application of one of the anisotropic failure criteria or by the application of continuum damage mechanics theories. Higher Order Theories have been proposed in attempt to improve the prediction of the stresses.

All of the equivalent single-layer theories share a common characteristic: the assumed distribution of the displacements through the thickness is continuous with the derivative with respect to the thickness coordinates. This implies that the out-of-plane shear strains are continuous across the material interfaces. As a result of the different material properties, the out-of-plane stress components are discontinuous at the interfaces between layers, thus violating the equilibrium conditions.

To overcome the limitations of the equivalent single-layer theories and to obtain a good evaluation of the stresses, a class of theories were developed. These theories are based on a distribution of displacements which is continuous in the thickness of the plate but with derivatives with respect to the thickness coordinates that are not necessarily continuous at the interfaces between layers. Layer-Wise Constant Shear (LCS) Theories were proposed by several authors [5-15]. The Finite Element implementation of these theories is not simple because they imply a large number of degrees of freedom (dof) per node. Moreover, the physical interpretations of the dof and the large number of stress resultants and displacements is not intuitive

Received September 1993
Revised January 1994

as in the CPT and FSDT. LCS Theories, for example, have not been used for shells because of the complexity of the formulation, except for the case of cylindrical shells [8].

Barbero [16] developed a new element for the analysis of laminated plates starting from the formulation done for three-dimensional shell elements by Ahmad *et al.* [17] and using the kinematic constraints of LCS Theories. In particular he noted that with the use of a 3D element, it is possible to analyze laminated composite plates overcoming the difficulties of LCS Theories but retaining the precise stresses calculation. However, in [16] the stresses were calculated by using only the constitutive equations. Here a procedure for the refined calculation of interlaminar stresses is developed along the lines of previous work [18-19]. The procedure requires computation of higher order derivatives of the shape functions. These derivatives are presented here in the context of the isoparametric formulation of three-dimensional problems.

The main disadvantage of conventional 3D continuum elements when utilized in the analysis of Composite Laminates Structures it is the large number of dof involved. The formulation presented here is based on the fact that certain assumptions made in the plate theories are quite valid for a broad class of problems of moderately thick laminates. The proposed element has a small number of dof per node and produces results as accurate as conventional 3D continuum elements for a large range of problems. With this element, the imposition of the boundary conditions, loads, etc., has a very simple physical interpretation and is identical to the conventional 3D continuum elements.

It is important to note that, because in this element the position of the middle surface is irrelevant, it is possible to model problems with a variable number of layers (ply drop-of), variable thickness (e.g. tapered glued-laminates, timber beams, etc.).

The objective of this work is to demonstrate the applicability of LCS Theories [5-15] to complex analysis problems of laminated structures (e.g., ply-drop-off). Specifically, this work is concerned with the development and validation of a 3-Dimensional Layer-wise Constant Shear (3DLCS) elements. From a designer's point of view, an important feature of the formulation presented here is that the loads, boundary conditions, and degrees of freedom have the same physical interpretation as in three-dimensional continuum elements. An interface with a commercial Finite Element Analysis (FEA) package (NISA) [20] was developed to further facilitate the interpretation of the results. Previous finite element implementations of LCS Theories, could not be efficiently incorporated in commercial FEA packages because of the large number of dof per node associated with two dimensional LCS Theories. The present three-dimensional formulation solves this problem completely. The interface with NISA demonstrates the case of implementation of the proposed element in commercial packages. Maximum accuracy in the computation of stresses is achieved in this work by postprocessing the stress results from constitutive equation with the aid of the equilibrium equation. The idea introduced in [18,19] for two dimensional elements is generalized here for three-dimensional elements. Validation of the present formulation is accomplished by the application of the patch test to laminated composites subjected to both in-plane loads and bending.

2. KINEMATICS AND CONSTITUTIVE EQUATIONS

Consider a laminated plate composed of n orthotropic laminae, each arbitrarily oriented with respect to the elemental coordinate (ξ, η, ζ). In particular ξ and η are two elemental coordinates in the middle plane of the plate element and ζ a linear coordinate in the thickness direction.

Each layer (or subset of layers) of the plate is discretized by the 3D elements. Pairs of points, i_{top} and i_{bottom}, each given in Cartesian coordinates, prescribe the shape of the element (Figure 1). If (ξ, η, ζ) vary between -1 and 1 on the respective faces of the element, a relationship between the Cartesian co-ordinate of any point of the plate and the elemental co-ordinate can be written in the form:

$$\begin{Bmatrix} x \\ y \\ z \end{Bmatrix} = \sum \overline{N}_i(\xi, \eta) \frac{(1+\zeta)}{2} \begin{Bmatrix} x_i \\ y_i \\ z_i \end{Bmatrix}_{top} + \sum \overline{N}_i(\xi, \eta) \frac{(1-\zeta)}{2} \begin{Bmatrix} x_i \\ y_i \\ z_i \end{Bmatrix}_{bottom} \tag{1}$$

where $\overline{N}_i(\xi, \eta)$ is a function taking a value of unity at the node i and zero at all other nodes.

The displacement $\{\mathbf{u}\} = \{u, v, w\}^T$ inside an element is given by:

$$\{\mathbf{u}\} = [\mathrm{N}]\{\boldsymbol{\delta}\} \tag{2}$$

where $\{\boldsymbol{\delta}\}$ is the collection of the nodal $\{\boldsymbol{\delta}_i\}$ that in this formulation is $\{\boldsymbol{\delta}_i\} = \{u_i; v_i; w_i\}^T$. The interpolation functions are equal for u, v and w:

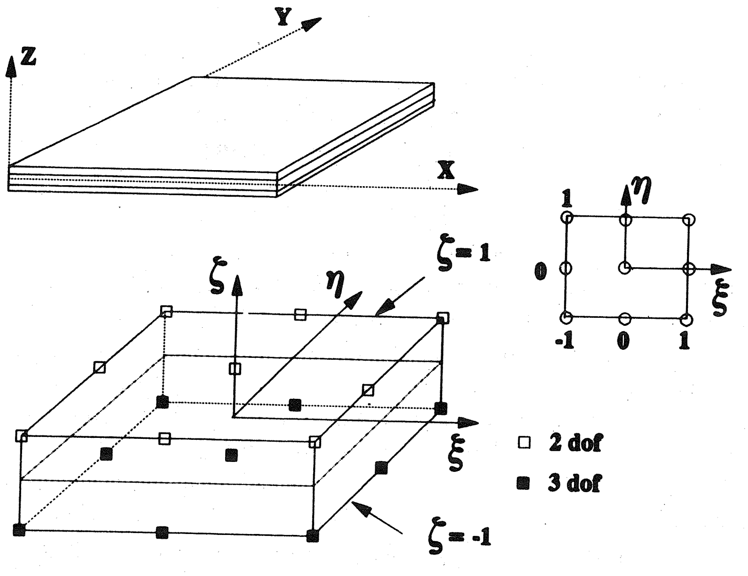

Figure 1. Plate geometry

$$\begin{Bmatrix} u \\ v \\ w \end{Bmatrix} = \sum_{i=1}^{n} \begin{bmatrix} N_i & 0 & 0 \\ 0 & N_i & 0 \\ 0 & 0 & N_i \end{bmatrix} \{ \delta_i \} \tag{3}$$

where n is the number of the nodes and $N_i = N_i\,(\xi, \eta, \zeta)$.

The order of interpolation functions N_i along the two directions on the surface of the plate can be chosen independently of the order through the thickness. Linear or quadratic interpolation of the displacements (u, v) and the geometry (x, y) are commonly used. The order of approximation in the thickness direction corresponds to different kinematical assumptions in LCS Theory. Here a linear variation is used. The quadratic element has 18 nodes. Nodes 1 to 9 have 3 dof (u, v and w), nodes 10 to 18 have 2 dof (u and v) as shown in Figure 2. The variables u and v correspond to the in-plane displacements at the interfaces between elements (layers). The transverse deflection w is constant through the thickness. Therefore, a single global node connects to all the local w-nodes that lie on a line perpendicular to the middle surface. The quadratic element has 45 dof.

The constitutive equations for the k-th layer made in orthotropic material arbitrarily oriented with respect to the global coordinates is similar to the equations for a monoclinic material [21].

Then we have, with reference to the local reference system (1, 2, 3) (Figure 3):

$$\begin{Bmatrix} \sigma'^k_1 \\ \sigma'^k_2 \\ \sigma'^k_3 \\ \sigma'^k_4 \\ \sigma'^k_5 \\ \sigma'^k_6 \end{Bmatrix} = \begin{bmatrix} C^k_{11} & C^k_{12} & C^k_{13} & 0 & 0 & 0 \\ C^k_{12} & C^k_{22} & C^k_{23} & 0 & 0 & 0 \\ C^k_{13} & C^k_{23} & C^k_{33} & 0 & 0 & 0 \\ 0 & 0 & 0 & C^k_{44} & 0 & 0 \\ 0 & 0 & 0 & 0 & C^k_{55} & 0 \\ 0 & 0 & 0 & 0 & 0 & C^k_{66} \end{bmatrix} \begin{Bmatrix} \varepsilon'^k_1 \\ \varepsilon'^k_2 \\ \varepsilon'^k_3 \\ 2\varepsilon'^k_4 \\ 2\varepsilon'^k_5 \\ 2\varepsilon'^k_6 \end{Bmatrix} \tag{4}$$

The two dimensional reduced stiffness matrix for an orthotropic material subjected to plane stress in local reference system is:

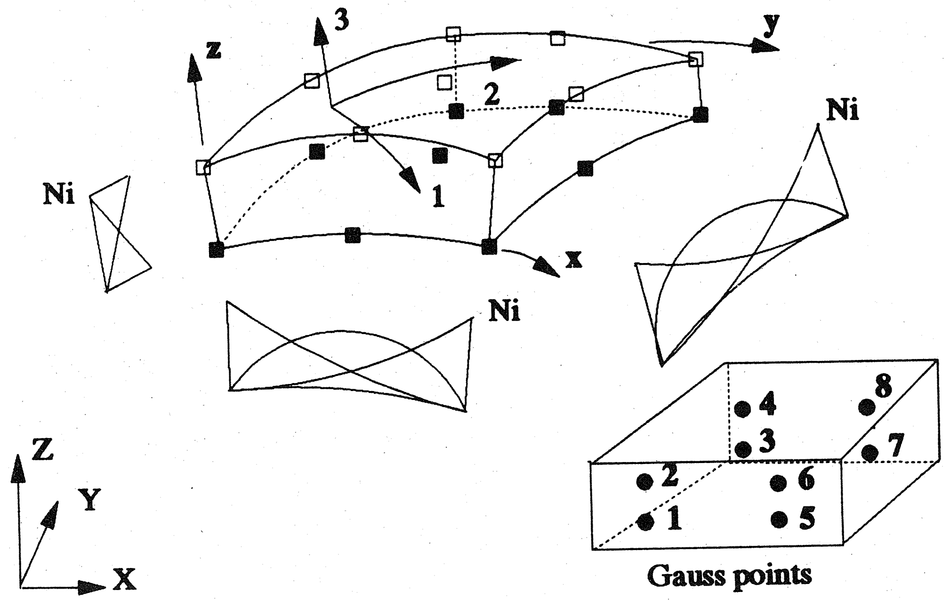

Figure 2. The 3DLCS element

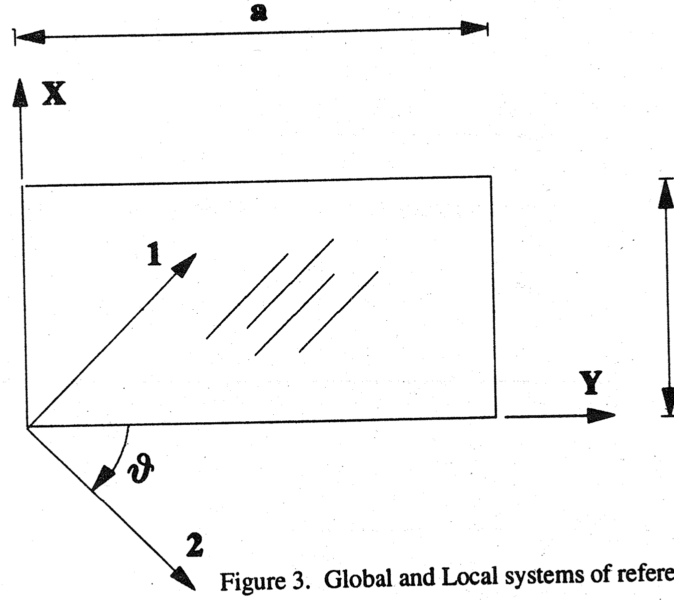

Figure 3. Global and Local systems of reference

$$\begin{Bmatrix} \sigma'^k_1 \\ \sigma'^k_2 \\ \sigma'^k_6 \end{Bmatrix} = \begin{bmatrix} Q^k_{11} & Q^k_{12} & 0 \\ Q^k_{12} & Q^k_{22} & 0 \\ 0 & 0 & Q^k_{66} \end{bmatrix} \begin{Bmatrix} \varepsilon'^k_1 \\ \varepsilon'^k_2 \\ 2\varepsilon'^k_6 \end{Bmatrix} \tag{5}$$

To overcome the locking effect that a vanishing transverse strain ($\varepsilon'^k_3 = 0$) would have, eqs. (4) and (5) are combined as follows,

$$[\overline{\mathbf{D}}^{\mathbf{k}}] = \begin{bmatrix} Q_{11}^k & Q_{12}^k & C_{13}^k & 0 & 0 & 0 \\ Q_{12}^k & Q_{22}^k & C_{23}^k & 0 & 0 & 0 \\ C_{13}^k & C_{23}^k & C_{33}^k & 0 & 0 & 0 \\ 0 & 0 & 0 & K^2 C_{44}^k & 0 & 0 \\ 0 & 0 & 0 & 0 & K^2 C_{55}^k & 0 \\ 0 & 0 & 0 & 0 & 0 & Q_{66}^k \end{bmatrix} \tag{6}$$

where K^2 is the shear correction factor fixed at the value of 5/6. In contracted notation we have:

$$\{ \sigma'^{\mathbf{k}} \} = [\overline{\mathbf{D}}^{\mathbf{k}}] \{ \varepsilon'^{\mathbf{k}} \} \tag{7}$$

The explicit expressions, in function of the Engineering constants, for the $[\overline{\mathbf{D}}]$ matrix coefficients are:

$$Q_{11}^k = \frac{E_1^k}{1 - \nu_{12}^k \nu_{21}^k}; \quad Q_{12}^k = \frac{\nu_{12}^k E_2^k}{1 - \nu_{12}^k \nu_{21}^k} = \frac{\nu_{21}^k E_1^k}{1 - \nu_{12}^k \nu_{21}^k}; \quad Q_{22}^k = \frac{E_2^k}{1 - \nu_{12}^k \nu_{21}^k};$$

$$C_{13}^k = \frac{\nu_{31}^k + \nu_{21}^k \nu_{32}^k}{E_2^k E_3^k \Delta^k} = \frac{\nu_{13}^k + \nu_{12}^k \nu_{23}^k}{E_1^k E_2^k \Delta^k}; \quad C_{23}^k = \frac{\nu_{32}^k + \nu_{12}^k \nu_{31}^k}{E_1^k E_3^k \Delta^k} = \frac{\nu_{23}^k + \nu_{21}^k \nu_{13}^k}{E_1^k E_2^k \Delta^k};$$

$$C_{33}^k = \frac{1 - \nu_{12}^k \nu_{21}^k}{E_1^k E_2^k \Delta^k}; \quad C_{44}^k = G_{23}^k; \quad C_{55}^k = G_{13}^k; \quad Q_{66}^k = G_{12}^k;$$

where:

$$\Delta^k = \frac{1 - \nu_{12}^k \nu_{21}^k - \nu_{23}^k \nu_{32}^k - \nu_{31}^k \nu_{13}^k - 2 \nu_{21}^k \nu_{32}^k \nu_{13}^k}{E_1^k E_2^k E_3^k}$$

The relationship between stress and strain written with reference to the global coordinate (x, y, z), and the rotation matrix for the lamina k is:

$$\{ \sigma^{\mathbf{k}} \} = [\mathbf{D}^{\mathbf{k}}] \{ \varepsilon^{\mathbf{k}} \} \tag{8}$$

where:

$$[\mathbf{D}^{\mathbf{k}}] = [\mathbf{T}^{\mathbf{k}}]^{-1} [\overline{\mathbf{D}}^{\mathbf{k}}] [\mathbf{T}^{\mathbf{k}}] \tag{9}$$

$$[\mathbf{T}^k] = \begin{bmatrix} \cos^2\theta^k & \sin^2\theta^k & 0 & 0 & 0 & 2\sin\theta^k\cos\theta^k \\ \sin^2\theta^k & \cos^2\theta^k & 0 & 0 & 0 & -2\sin\theta^k\cos\theta^k \\ 0 & 0 & 1 & 0 & 0 & 0 \\ 0 & 0 & 0 & \cos\theta^k & -\sin\theta^k & 0 \\ 0 & 0 & 0 & \sin\theta^k & \cos\theta^k & 0 \\ -\sin\theta^k\cos\theta^k & \sin\theta^k\cos\theta^k & 0 & 0 & 0 & \cos^2\theta^k - \sin^2\theta^k \end{bmatrix} \tag{10}$$

The components in directions of orthogonal axes related to the surface $\zeta = constant$ are essential if account is to be taken of the kinematic assumptions of LCS Theory. The strain components of interest are:

$$\{ \varepsilon \} = \begin{Bmatrix} \varepsilon_x \\ \varepsilon_y \\ \gamma_{yz} \\ \gamma_{xz} \\ \gamma_{xy} \end{Bmatrix} = \begin{Bmatrix} u,_x \\ v,_y \\ w,_y + v,_z \\ w,_x + u,_z \\ u,_y + v,_x \end{Bmatrix} \tag{11}$$

with the strain in direction z neglected so as to be consistent with the plate LCS Theory assumption of incompressibility of normals. Here and in the following, comma indicates a derivative with respect to the indicated coordinate.

3. INTEGRATION OF THE PLATE STIFFNESS MATRIX

The total potential energy Π, can be expressed as:

$$\Pi = \frac{1}{2}\int_V \{\,\sigma\,\}^T\{\,\varepsilon\,\}\,dV - \int_V \{\,\mathbf{u}\,\}^T\{\,\mathbf{p}\,\}\,dV - \int_S \{\,\mathbf{u}\,\}^T\{\,\mathbf{q}\,\}\,dS \tag{12}$$

where $\{\,\sigma\,\}$ and $\{\,\varepsilon\,\}$ are the stress and the strain vectors respectively, $\{\,\mathbf{u}\,\}$ the displacements at any point, $\{\,\mathbf{p}\,\}$ the body forces per unit volume and $\{\,\mathbf{q}\,\}$ the applied surface tractions. Integrations are taken over the volume V of the structure and loaded area S. The first term on the right hand of (12) represents the internal strain energy and the second and third terms are, respectively, the work of the body forces and distribute surface loads. Replacing eqs. (2) and (8) into (12) and considering that with the Finite Element Analysis (FEA) the total potential energy of a continuum will be the sum of the energy contributions of the individual element in which the structure has been divided, we can write the total potential energy of the element e as follows:

$$\Pi_e = \frac{1}{2}\int_{V_e} \{\,\delta^{\mathbf{e}}\,\}^{\mathrm{T}}[\mathbf{B}]^T[\mathbf{D}]\,[\mathbf{B}]\,\{\,\delta^{\mathbf{e}}\,\}\,dV - \int_{V_e} \{\,\delta^{\mathbf{e}}\,\}^T[\mathbf{N}]^T\{\,\mathbf{p}\,\}\,dV_e - \int_{S_e} \{\,\delta^{\mathbf{e}}\,\}^T[\mathbf{N}]^T\;\{\,\mathbf{q}\,\}\,dS_e \tag{13}$$

where V_e is the element volume, S_e the elemental loaded surface area, $\{\,\delta^{\mathbf{e}}\,\}$ is the vector of nodal displacements of the element and $[\mathbf{B}]$ is the strain matrix, composed of derivatives of the shape functions written with respect to the coordinates (x, y, z) and correlating strains and $\{\,\delta^{\mathbf{e}}\,\}$ as:

$$\{\,\varepsilon\,\} = [\mathbf{B}]\,\{\,\delta^{\mathbf{e}}\,\} \tag{14}$$

The minimization of the Total Potential Energy, with respect to the nodal displacements $\{\,\delta^{\mathbf{e}}\,\}$ results in:

$$\frac{\partial\,\Pi^e}{\partial\,\{\,\delta^{\mathbf{e}}\,\}} = \left[\int_{V_e} [\mathbf{B}]^T[\mathbf{D}]\,[\mathbf{B}]\,dV_e\right]\{\,\delta^{\mathbf{e}}\,\} - \left\{\int_{V_e} [\mathbf{N}]^T\{\,\mathbf{p}\,\}\,dV_e + \int_{S_e} [\mathbf{N}]^T\{\,\mathbf{q}\,\}\,dS_e\right\} = [\,\mathbf{K}^{\mathbf{e}}\,]\{\,\delta^{\mathbf{e}}\,\} - \{\,\mathbf{F}^{\mathbf{e}}\,\} = 0 \tag{15}$$

where $\{\,\mathbf{F}^{\mathbf{e}}\,\}$ is the equivalent nodal force vector and $[\mathbf{K}^{\mathbf{e}}]$ is the stiffness matrix period.

The stiffness matrix is written as (with third row and column of $[\mathbf{D}]$ deleted):

$$[\,\mathbf{K}^{\mathbf{e}}\,] = \int_V [\mathbf{B}]^T[\mathbf{D}]\,[\mathbf{B}]\,dx\,dy\,dz \tag{16}$$

The matrix $\mathbf{B}$ can be written explicitily as:

$$[\mathbf{B}] = \begin{bmatrix} \ldots N_{i,x} & 0 & 0\ldots \\ \ldots 0 & N_{i,y} & 0\ldots \\ \ldots 0 & N_{i,z} & N_{i,y}\ldots \\ \ldots N_{i,z} & 0 & N_{i,x}\ldots \\ \ldots N_{i,y} & N_{i,x} & 0\ldots \end{bmatrix} \tag{17}$$

The layer-wise constant shear constraint is satisfied by virtue of the linearity through the thickness of the displacements u and v in eq. (2) (Figure 2). The incompressibility of the normals is imposed by omitting ε_z in eqs. (11) and (17).

The derivative of the displacements with respect to the global axes (x, y, z) are obtained in the standard way as:

$$\begin{bmatrix} u_{,x} & v_{,x} & w_{,x} \\ u_{,y} & v_{,y} & w_{,y} \\ u_{,z} & v_{,z} & w_{,z} \end{bmatrix} = [\mathbf{J}]^{-1} \begin{bmatrix} u_{,\xi} & v_{,\xi} & w_{,\xi} \\ u_{,\eta} & v_{,\eta} & w_{,\eta} \\ u_{,\zeta} & v_{,\zeta} & w_{,\zeta} \end{bmatrix} \tag{18}$$

The Jacobian matrix is defined as:

$$[\mathbf{J}] = \begin{bmatrix} x_{,\xi} & y_{,\xi} & z_{,\xi} \\ x_{,\eta} & y_{,\eta} & z_{,\eta} \\ x_{,\zeta} & y_{,\zeta} & z_{,\zeta} \end{bmatrix} \tag{19}$$

and is calculated from the coordinate definition of equation (1).

Eq. (16) can be used directly to assemble the global stiffness matrix. The assembly procedure and the boundary conditions are described in section 4.

The numerical integration is performed by Gaussian quadrature [22]. A two point rule suffices in the ζ direction, while a minimum of three or four points in both ξ and η directions is needed for parabolic or cubic elements respectively. Reduced integration is used in the ξ and η directions for the shear terms.

The loads can be defined in the global coordinate system. If pressure is applied the calculation of the loaded area in the global coordinate is necessary and the nodal forces can be obtained by the knowledge of the Jacobian and the element thickness, by the following relation:

$$\{\mathbf{F_p}\} = \int_A [\mathbf{N}] \begin{bmatrix} P_x \\ P_y \\ P_z \end{bmatrix} dA = \sum_{r=1}^{ngp} \sum_{s=1}^{ngp} \begin{bmatrix} N_i P_x \\ N_i P_y \\ N_i P_z \end{bmatrix} W_{\xi_r} W_{\eta_s} |J|_{\xi_r, \eta_s} \frac{2}{TH} \tag{20}$$

where:

- P_i is the component of the distributed load in the direction i;
- A is the area of upper, or middle or bottom surface of the 3DLCS element, depending on the position of the loading;
- TH is the thickness of the 3DLCS element of each Gaussian point (ngp = number of Gaussian points);
- W is the weight at each Gaussian point;
- ζ is equal to 1 or – 1 or 0 respectively when the distributed loading is on upper or bottom or middle surface.

4. ASSEMBLY PROCEDURE AND CONDENSATION OF REDUNDANT dof

The integration of the element stiffness matrix is performed as a standard 18-node element with 3 dof per node (u, v, w) but with the appropriate shape functions N_i described previously (Figure 2).

The transverse deflection w is constant through the thickness of the element by the incompressibility assumption made omitting ε_z in eqs. (11) and (17). Therefore, the dof of two nodes aligned through the thickness of an element can be reduced to a single dof (w in the bottom for example). If this is not done the stiffness matrix present a singularity and the solution cannot be reached.

Then, at the element level the stiffness matrix is rearranged so that the dof corresponding to the displacement u and v on the surface of the plate for all nodes (e.g. 18 nodes) are considered first.

The remaining dof corresponding to w-displacements are assigned to a new set of nodes (e.g. 9 nodes) called w-master nodes in this work. The w-master nodes are independent of the original nodes to facilitate the assembly procedure. However, they can be any set of nodes located at one of the interfaces of the laminate. The location of the w-nodes through the thickness of the laminate does not affect the results. At the element level, the resulting element has 18 nodes with 2 dof (u and v) per node plus nine additional nodes with 1 dof (w) per node.

If more than one layer is present in the laminate, another condensation procedure must be done for each vertical in which we assume that the w-displacements are equal, due to the incompressibility condition, and then only one w-master node (e.g.: the w-master node at the bottom of the laminate) must be taken into account, connecting the remaining node to this master node. This has been easily achieved through the usual assembly by assigning the same global node number of the w-master node to all the w-nodes located on its normal.

The technique adopted has the following advantages:

(a) eliminates the need for complex bookkeeping to identify individual sets of elements stacked to form a laminate.
(b) allows the front-width of the band-width optimization algorithm to take into account the thickness direction as well as the surface direction in the search for the optimum element or node assembly order.
(c) eliminates the need for elements with a large dof number that otherwise results if the assembly through the thickness is performed a priori. This is particularly useful for implementation in commercial FEA codes [23].

5. REFINED COMPUTATION OF STRESSES

The constitutive equations (7) are used to obtain all six components of stress at the reduced Gauss points. The distribution of in-plane stresses σ_x, σ_y and σ_{xy} is linear through the thickness. The distribution of inter-laminar stresses σ_{xz} and σ_{yz} is layer-wise constant. All components of stress obtained at the integration points can be extrapolated to the nodes using the procedure described by Cook in 1974 [22]. This is done to facilitate the graphic output using pre- and post- processing package [20].

Selective reduced integration is used on the shear-related terms. The new element (3DLCS) reduces to FSDT when only one element is used through the thickness. Therefore, the behaviour of the 9-node Lagrangian FSDT element with selective reduced integration, free of shear locking, is also present in the proposed element. Furthermore, Reddy and Barbero [23] successfully used selective reduced integration on their LCST element that has the same kinematic as a stack of 3DLCS elements. As shown by Averil [24], the 9-node Lagrangian element with selective reduced integration does not exhibit locking as the plate (or, in this paper, layer) becomes very thin. This is a remarkable advantage of the proposed element over conventional 3-D continuum elements with full integration.

The 3DLCS element gives a very good representation of all the stress components except σ_z without the aspect ratio limitations of conventional 3-D continuum elements. When transverse stress σ_z is needed, either conventional 3-D continuum elements can be used or further postprocessing can be done by using the third equilibrium equation:

$$\frac{\partial \sigma_{xz}}{\partial x} + \frac{\partial \sigma_{yz}}{\partial y} + \frac{\partial \sigma_z}{\partial z} + p_z = 0 \tag{21}$$

Quadratic interlaminar stresses that satisfy the shear boundary conditions at the top and at bottom surfaces of the plate are obtained in this work for laminated plates modelled with 3DLCS elements. An approximation of the shear stress distribution through each layer with a quadratic function requires $3n$ equations for each of the shear stresses (σ_{xz}, σ_{yz}), where n is the number of layers. To obtain these $3n$ equations, Chaudhuri [18] proposed that n equations can be used to satisfy the n average shear stresses on each layer, two equations can be used to impose vanishing shear stresses at the surface of the plate (top and bottom), $(n-1)$ equations are needed to satisfy the continuity of the shear stresses at the interfaces between layers and the remaining $(n-1)$ equations has to be used to compute the jump in $\sigma_{xz,z}$ (or $\sigma_{yz,z}$) at each interface.

The average shear stresses on each layer are computed from the constitutive equations and the displacement field obtained in the FEA.

In this work, the following equilibrium equations

$$\frac{\partial \sigma_{xz}}{\partial z} = -\left(\frac{\partial \sigma_x}{\partial x} + \frac{\partial \sigma_{xy}}{\partial y}\right); \qquad \frac{\partial \sigma_{yz}}{\partial z} = -\left(\frac{\partial \sigma_{xy}}{\partial x} + \frac{\partial \sigma_y}{\partial y}\right) \tag{22}$$

are used to compute $\sigma_{xz,z}$ and $\sigma_{yz,z}$ directly from the FEA approximation in the proposed element.

The procedure requires computation of second derivatives of the displacement (u, v, w). In this work, the second derivatives are obtained from the shape functions used in the isoparameteric formulation (Appendix II).

Using eqs. (8), (14) and (17) we can write:

$$\begin{Bmatrix} \sigma^k_{x,x} \\ \sigma^k_{y,x} \\ \sigma^k_{yz,x} \\ \sigma^k_{xz,x} \\ \sigma^k_{xy,x} \end{Bmatrix} = [\mathbf{D^k}] \begin{bmatrix} \ldots N_{i,xx} & 0 & 0\ldots \\ \ldots 0 & N_{i,yx} & 0\ldots \\ \ldots 0 & N_{i,zx} & N_{i,yx}\cdots \\ \ldots N_{i,zx} & 0 & N_{i,xx}\cdots \\ \ldots N_{i,yx} & N_{i,xx} & 0\ldots \end{bmatrix} \{ \delta^e \} = [\mathbf{D^k}]\,[\mathbf{B_x}]\,\{ \delta^e \} \tag{23}$$

and similarly:

$$\begin{Bmatrix} \sigma^k_{x,y} \\ \sigma^k_{y,y} \\ \sigma^k_{yz,y} \\ \sigma^k_{xz,y} \\ \sigma^k_{xy,y} \end{Bmatrix} = [\mathbf{D^k}] \begin{bmatrix} \ldots N_{i,xy} & 0 & 0\ldots \\ \ldots 0 & N_{i,yy} & 0\ldots \\ \ldots 0 & N_{i,zy} & N_{i,yy}\cdots \\ \ldots N_{i,zy} & 0 & N_{i,xy}\cdots \\ \ldots N_{i,yy} & N_{i,xy} & 0\ldots \end{bmatrix} \{ \delta^e \} = [\mathbf{D^k}]\,[\mathbf{B_y}]\,\{ \delta^e \} \tag{24}$$

where the matrices $[\mathbf{B_x}]$ and $[\mathbf{B_y}]$ are used for the computation of the second derivatives of stresses in the same way as the strain-displacement matrix $[\mathbf{B}]$ is used for the computation of stresses. With the second derivatives of stresses, the parabolic shape of σ_{xz} and σ_{yz} through the thickness with respect to the local axes can be obtained. Then, by the knowledge of the angle θ between the local axes and the natural directions (1, 2, 3) (Figure 2) it is possible to calculate the stresses in direction of the fibres and normal to them, which are needed to study the failure or damage of laminated, composite plates.

6. VALIDATION

6.1. Patch tests

As originally conceived by Iron [25, 26], the patch test simply verifies that an arbitrary *patch* of assembled elements reproduces exactly the behaviour of an elastic solid material when subjected to boundary displacements consistent with constant straining.

By numerous publications it was shown that:

(a) the patch test still remains a *necessary* condition for the finite element form;
(b) it can be readily extended to check *sufficient* requirements for convergence;
(c) is an assessment of the asymptotic convergence rate of a particular finite element form;
(d) is useful to check the robustness of the appropriate algorithm which violate in their formulation the compatibility (continuity) requirements.

Figures 4 and 5 show acceptable *patch test* [25, 26] meshes to validate the proposed element. Boundary nodes of the *patches* are loaded by consistently derived nodal loads appropriate to state of constant strain/stress. Internal nodes are neither loaded nor restrained. The *patches* are provided with enough support to prevent a rigid-body motion. The standard finite element procedure is executed and the computed stresses, strains and the displacements are compared with the exact solution. If these values are the same or the difference is an acceptable tolerance then the *patch tests* are passed. Application to laminated composites under traction and bending is shown next.

6.1.1. Patch test on an isotropic plate under in-plane loading

An isotropic plate under in-plane loading was analysed with the five element mesh depicted in Figure 4.

The in-plane stress is taken to be unity and the material adopted has these mechanical parameters:

$$E = 29000\ K\,si\,; \qquad \nu = 0.294$$

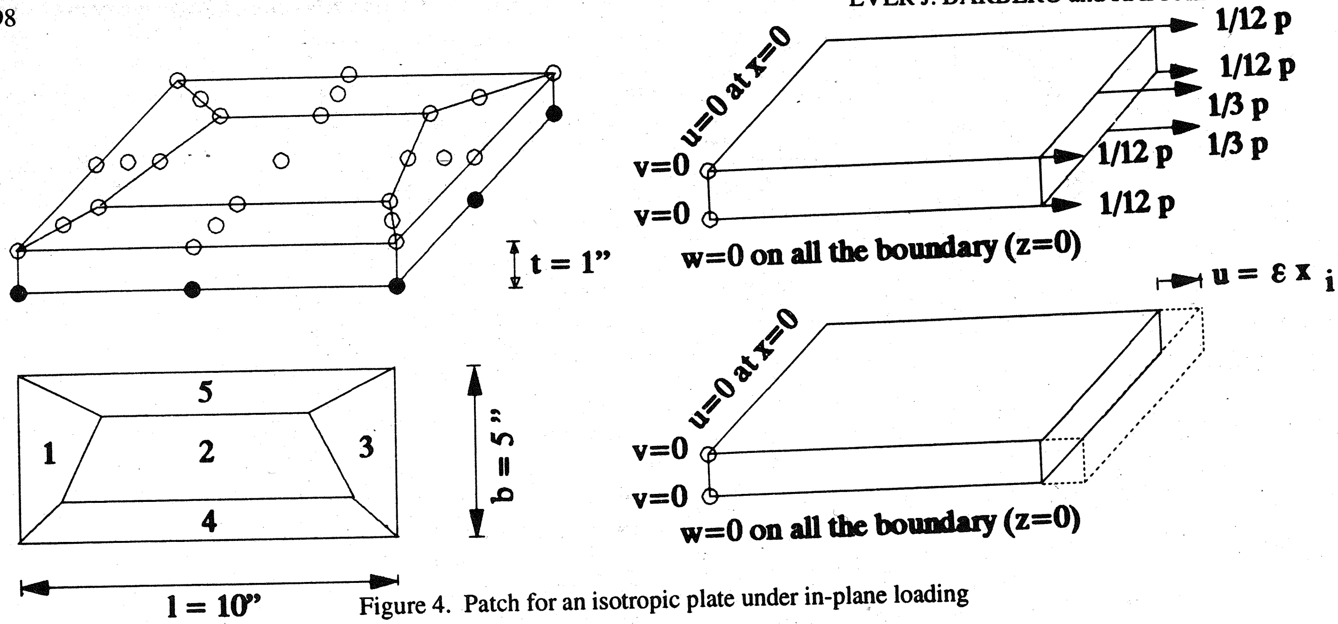

Figure 4. Patch for an isotropic plate under in-plane loading

Then the exact solution for the stress and the strain is:

$$\sigma_x = 1.0\,Ksi\,; \qquad \varepsilon_x = \frac{1}{E} = 3.44827 \times 10^{-5}\,; \qquad \varepsilon_y = \frac{-\nu}{E} = -\,1.014 \times 10^{-5}$$

In all the five elements and in each Gauss point the values computed by the FEA coincide with the expected solution. The same *patch test* was performed by applying the specified displacements u at the free face ($l = 10.00''$) calculated by the relation:

$$u = \int_0^l \varepsilon_x\,dx = \varepsilon_x\,l = 10 \times 3.44827 \times 10^{-5} = 3.44827 \times 10^{-4}$$

and the same results are reached.

6.1.2. Patch test on a composite laminated plate under in-plane loading

A second patch test, similar to the previous, but on a three layers laminate (0°/90°/0°), is performed to check the proposed 3DLCS element. The material adopted has these mechanical parameters:

$$E_1 = 3.0\,GPa; \quad E_2 = E_3 = 1.0\,GPa; \quad G_{12} = G_{13} = G_{23} = 0.5\,GPa; \quad \nu_{12} = \nu_{13} = \nu_{23} = 0.25$$

The patch is firstly loaded by consistently derived forces to have a unitary distributed load on the loaded faces. Then the same patch is subjected to the uniform displacement on the free faces $l = 10.0''$ in a way to produce the same unitary distribution on the loaded face. The dimensions and labels of the elements and layers are shown in Figure 5 while the boundary conditions are the same as example 6.1.1.

The exact solution is obtained by a simple computer program based on the Classical Laminate Theory [21]. In particular, the displacements u_i and v_i at the nodal points are calculated by:

$$u_i = \int_0^{x_i} \varepsilon_x\,dx = x_i\,\varepsilon_x\,; \quad v_i = \int_0^{y_i} \varepsilon_y\,dy = y_i\,\varepsilon_y$$

The results are shown in Tables 1 to 6.

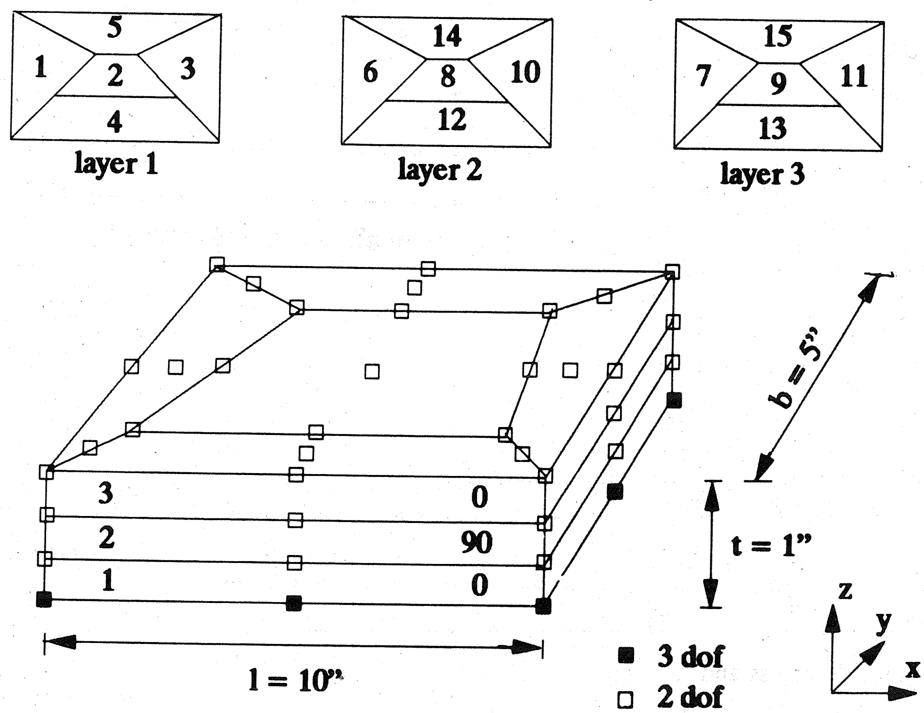

Figure 5. Patch for a laminate under in-plane loading

Table 1. Stresses and Strains at the Gauss Points of the element no. 1 - Specified displacements

G.P.	$\sigma_x\ (GPa)$		$\sigma_y \cdot 10\ (GPa)$		ε_x		$\varepsilon_y \cdot 10$	
num.	*C.P.T*	*3DLCS*	*C.P.T.*	*3DLCS*	*C.P.T.*	*3DLCS*	*C.P.T.*	*3DLCS*
1	1.290	1.288	0.436	0.463	0.426	0.426	− 0.640	− 0.610
2	1.290	1.288	0.436	0.435	0.426	0.426	− 0.640	− 0.638
3	1.290	1.288	0.436	0.392	0.426	0.426	− 0.640	− 0.680
4	1.290	1.289	0.436	0.435	0.426	0.426	− 0.640	− 0.639
5	1.290	1.289	0.436	0.444	0.426	0.426	− 0.640	− 0.629
6	1.290	1.289	0.436	0.435	0.426	0.426	− 0.640	− 0.638
7	1.290	1.289	0.436	0.449	0.426	0.426	− 0.640	− 0.624
8	1.290	1.289	0.436	0.434	0.426	0.426	− 0.640	− 0.639

Table 2. Stresses and Strains in the Gauss Points of the element no. 6 - Specified displacements

G.P.	$\sigma_x\ (GPa)$		$\sigma_y \cdot 10\ (GPa)$		ε_x		$\varepsilon_y \cdot 10$	
num.	*C.P.T*	*3DLCS*	*C.P.T.*	*3DLCS*	*C.P.T.*	*3DLCS*	*C.P.T.*	*3DLCS*
1	0.419	0.418	− 0.871	− 0.902	0.426	0.426	− 0.640	− 0.649
2	0.419	0.418	− 0.871	− 0.902	0.426	0.426	− 0.640	− 0.649
3	0.419	0.419	− 0.871	− 0.824	0.426	0.426	− 0.640	− 0.623
4	0.419	0.419	− 0.871	− 0.824	0.426	0.426	− 0.640	− 0.623
5	0.419	0.419	− 0.871	− 0.878	0.426	0.426	− 0.640	− 0.642
6	0.419	0.419	− 0.871	− 0.878	0.426	0.426	− 0.640	− 0.642
7	0.419	0.419	− 0.871	− 0.890	0.426	0.426	− 0.640	− 0.646
8	0.419	0.419	− 0.871	− 0.890	0.426	0.426	− 0.640	− 0.646

Table 3. Stresses and Strains at the Gauss Points of the element no. 1 - Patch subjected to forces

G.P.	σ_x (GPa)		$\sigma_y \cdot 10$ (GPa)		ε_x		$\varepsilon_y \cdot 10$	
num.	C.P.T	3DLCS	C.P.T.	3DLCS	C.P.T.	3DLCS	C.P.T.	3DLCS
1	1.290	1.288	0.436	0.457	0.426	0.425	−0.640	−0.616
2	1.290	1.292	0.436	0.429	0.426	0.427	−0.640	−0.647
3	1.290	1.290	0.436	0.394	0.426	0.427	−0.640	−0.680
4	1.290	1.291	0.436	0.431	0.426	0.427	−0.640	−0.645
5	1.290	1.281	0.436	0.424	0.426	0.423	−0.640	−0.644
6	1.290	1.298	0.436	0.442	0.426	0.429	−0.640	−0.639
7	1.290	1.282	0.436	0.438	0.426	0.425	−0.640	−0.630
8	1.290	1.297	0.436	0.442	0.426	0.429	−0.640	−0.639

Table 4. Stresses and Strains in the Gauss Points of the element no. 6 - Patch subjected to forces

G.P.	σ_x (GPa)		$\sigma_y \cdot 10$ (GPa)		ε_x		$\varepsilon_y \cdot 10$	
num.	C.P.T	3DLCS	C.P.T.	3DLCS	C.P.T.	3DLCS	C.P.T.	3DLCS
1	0.419	0.420	−0.871	−0.926	0.426	0.427	−0.640	−0.640
2	0.419	0.420	−0.871	−0.926	0.426	0.427	−0.640	−0.640
3	0.419	0.420	−0.871	−0.847	0.426	0.428	−0.640	−0.560
4	0.419	0.420	−0.871	−0.847	0.426	0.426	−0.640	−0.560
5	0.419	0.424	−0.871	−0.854	0.426	0.428	−0.640	−0.600
6	0.419	0.424	−0.871	−0.854	0.426	0.426	−0.640	−0.600
7	0.419	0.424	−0.871	−0.869	0.426	0.425	−0.640	−0.590
8	0.419	0.424	−0.871	−0.869	0.426	0.429	−0.640	−0.590

Table 5. Stresses at the centre of the elements

	Applied forces				*Specified displacements*			
Element	σ_x (GPa)		$\sigma_y \cdot 10$ (GPa)		σ_x (GPa)		$\sigma_y \cdot 10$ (GPa)	
num.	C.P.T.	3DLCS	C.P.T.	3DLCS	C.P.T.	3DLCS	C.P.T.	3DLCS
1	1.290	1.289	0.436	0.436	1.290	1.289	0.436	0.432
2	1.290	1.289	0.436	0.416	1.290	1.289	0.436	0.421
3	1.290	1.289	0.436	0.436	1.290	1.283	0.436	0.417
4	1.290	1.289	0.436	0.395	1.290	1.291	0.436	0.396
5	1.290	1.289	0.436	0.399	1.290	1.291	0.436	0.400
6	0.419	0.419	−0.871	−0.873	0.419	0.422	−0.871	−0.874
7	1.290	1.289	0.436	0.436	1.290	1.290	0.436	0.432
8	0.419	0.419	−0.871	−0.833	0.419	0.422	−0.871	−0.828
9	1.290	1.289	0.436	0.416	1.290	1.289	0.436	0.421
10	0.419	0.419	−0.871	−0.873	0.419	0.437	−0.871	−0.854

(Contd.)

Table 5 (Contd.)

11	1.290	1.289	0.436	0.436	1.290	1.282	0.436	0.417
12	0.419	0.419	−0.871	−0.791	0.419	0.421	−0.871	−0.791
13	1.290	1.289	0.436	0.395	1.290	1.291	0.436	0.396
14	0.419	0.419	−0.871	−0.800	0.419	0.420	−0.871	−0.795
15	1.290	1.289	0.436	0.399	1.290	1.291	0.436	0.400

Table 6. Displacements at the nodes ε_x (*C.P.T*) = 0.426 ε_y (*C.P.T*) = − 0.064)

	Coordinate		*C.P.T.*		*Applied forces*		*Specified displace.*	
node	*x*	*y*	*u*	*v*	*u*	*v*	*u*	*v*
1	0.000	0.000	0.000	0.000	0.000	0.000	0.000	0.000
2	2.000	1.667	0.852	−0.107	0.859	−0.103	0.852	−0.104
3	3.000	3.333	1.278	−0.213	1.284	−0.220	1.278	−0.217
4	0.000	5.000	0.000	−0.320	0.000	−0.342	0.000	−0.340
5	1.000	0.833	0.426	−0.053	0.421	−0.060	0.426	−0.058
6	2.500	2.500	1.065	−0.160	1.054	−0.160	1.065	−0.160
7	1.500	4.167	0.639	−0.267	0.636	−0.267	0.639	−0.265
8	0.000	2.500	0.000	−0.160	0.000	−0.157	0.000	−0.156
9	8.000	1.667	3.408	−0.107	3.408	−0.103	3.407	−0.104
10	7.000	3.333	2.982	−0.213	2.964	−0.220	2.981	−0.217
11	5.000	1.667	2.130	−0.107	2.133	−0.107	2.130	−0.103
12	5.000	3.333	2.130	−0.213	2.136	−0.219	2.130	−0.218
13	10.000	0.000	4.260	0.000	4.224	0.004	4.260	0.003
14	10.000	5.000	4.260	−0.320	4.220	−0.342	4.260	−0.339
15	9.000	0.833	3.834	−0.053	3.847	−0.059	3.835	−0.059
16	10.000	2.500	4.260	−0.160	4.168	−0.155	4.260	−0.156
17	8.500	4.167	3.621	−0.267	3.643	−0.269	3.621	−0.265
18	5.000	0.000	2.130	0.000	2.143	0.025	2.130	0.026
19	5.000	5.000	2.130	−0.320	2.142	−0.344	2.130	−0.341
20	1.250	2.500	0.533	−0.160	0.536	−0.161	0.533	−0.158
21	8.750	2.500	3.728	−0.160	3.757	−0.163	3.727	−0.159
22	5.000	0.833	2.130	−0.053	2.134	−0.056	2.130	−0.054
23	5.000	4.167	2.130	−0.267	2.133	−0.264	2.130	−0.262
24	5.000	2.500	2.130	−0.160	2.143	−0.164	2.130	−0.160

6.1.3. Patch test on an isotropic plate under constant curvature

A patch of an isotropic plate with material properties of example 6.1.1 is subjected to a constant curvature $\chi_x = 10^{-6}$ along the x axis. Figure 6 shows dimensions, labels and boundary conditions of this patch test. The strains ε_x at the Gauss points can be calculated by:

$$\varepsilon_x = \chi_x \cdot z_G = 1 \times 10^{-6} \times (\pm\ 0.289) \times t = \pm\ 0.289 \times 10^{-6}$$

where the coordinate z is zero at the middle surface of the plate. The FEA solution perfectly reproduces the *C.P.T.* values. The values of γ_{xz} are zero everywhere in perfect agreement with the hypotheses of the *C.P.T.*

6.1.4. Patch test on a composite laminated plate under constant curvature

The same patch used in example 6.1.2 (Figure 5) is now subjected to a constant curvature χ_x fixed at the value of 1×10^{-6} as in the previous example. The curvature has been obtained fixing, at the side $x = \pm\ 5.0''$ (origin of the axes fixed at the centre of the middle plane), the nodal displacements given by:

$$\bar{u}_i = \varepsilon_x \cdot x_i = \chi_x \cdot z_i \cdot x_i$$

The remaining boundary conditions are the same of example 6.1.3.

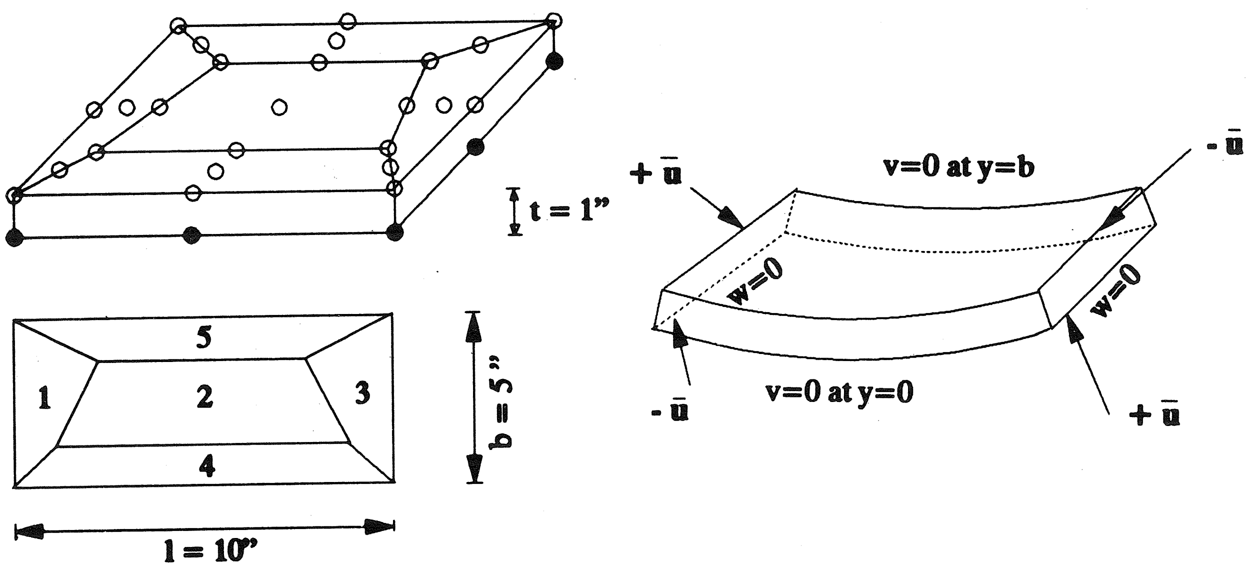

Figure 6. Patch for an isotropic plate under constant curvature

The comparisons between the results obtained by the proposed 3DLCS element and the C.P.T are shown in Table 7 and 8. The shear strain γ_{zx} obtained by the FEA is zero in each Gauss Point as hypotized in the C.P.T. By the comparison of the results obtained, shown in table 1 to 8, we can affirm that the patch test is passed. The differences regarding the effects in direction y are indicative of a better representation by the 3DLCS element of the real 3D state of stresses and deformation as compared to C.P.T. and not a deficiency of the element in passing the patch test.

Table 7. Stresses σ_x at the nodes . T1 (T2) Top of layer 1 (2) – B1 (B2) Bottom of layer 1 (2)

	Element 1 $\sigma_x \cdot 10^5$ *(GPa)*			*Element* 6 $\sigma_x \cdot 10^5$ *(GPa)*		
node	*pos.*	*3DLCS*	*C.P.T*	*pos.*	*3DLCS*	*C.P.T*
1	B1	0.153	0.150	B2	0.017	0.016
2	B1	0.153	0.150	B2	0.017	0.016
3	B1	0.153	0.150	B2	0.017	0.016
4	B1	0.153	0.150	B2	0.017	0.016
5	B1	0.153	0.150	B2	0.017	0.016
6	B1	0.153	0.150	B2	0.017	0.016
7	B1	0.153	0.150	B2	0.017	0.016
8	B1	0.153	0.150	B2	0.017	0.016
10	T1	0.051	0.050	T2	−0.017	−0.016
11	T1	0.051	0.050	T2	−0.017	−0.016
12	T1	0.051	0.050	T2	−0.017	−0.016
13	T1	0.051	0.050	T2	−0.017	−0.016
14	T1	0.051	0.050	T2	−0.017	−0.016
15	T1	0.051	0.050	T2	−0.017	−0.016
16	T1	0.051	0.050	T2	−0.017	−0.016
17	T1	0.051	0.050	T2	−0.017	−0.016

Table 8. Strains $\varepsilon_x \cdot 10^6$ at the Gauss Points of elements no. 1 and no. 6

	Element no. 1		*Element no.* 6	
G.P.	*3DLCS*	*C.P.T.*	*3DLCS*	*C.P.T*
1	0.42956	0.42955	0.09622	0.09623
2	0.23710	0.23711	−0.09622	−0.09623
3	0.42956	0.42955	0.09623	0.09623
4	0.23711	0.23711	−0.09623	−0.09623
5	0.42956	0.42955	0.09623	0.09623
6	0.23711	0.23711	−0.09623	−0.09623
7	0.42956	0.42955	0.09623	0.09623
8	0.23711	0.23711	−0.09623	−0.09623

6.2. Refined computation of stresses

Next we consider a case of a simply-supported (0°/90°/0°) square ($l \cdot l$) plate under uniformly distributed transverse load. The material properties are:

$$E_1 = 19.2 \times 10^6 \text{ psi}; \quad E_2 = E_3 = 1.56 \times 10^6 \text{ psi}; \quad G_{12} = G_{13} = 0.82 \times 10^6 \text{ psi}$$

$$G_{23} = 0.523 \times 10^6 \text{ psi}; \quad \nu_{12} = \nu_{13} = 0.24; \quad \nu_{23} = 0.49$$

The plate is simply-supported on all four sides. Owing the symmetry, only a quarter of the plate is modelled by a $4 \times 4 \times 3$ mesh of 3DLCS elements. Figure 7 shows the dimensions and the boundary conditions adopted.

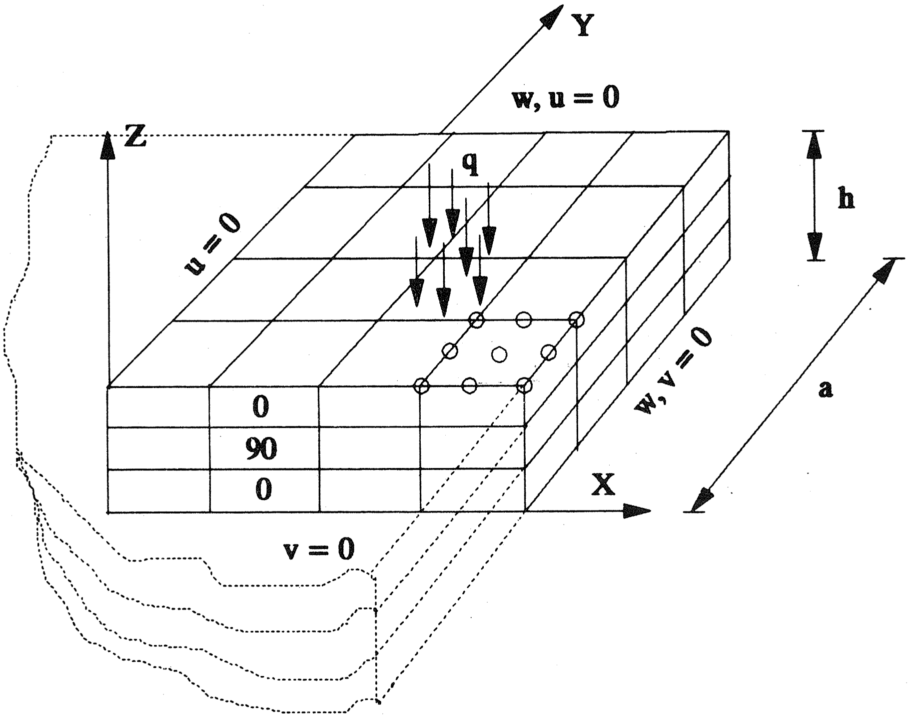

Figure 7 - Scheme used for the computation of the stresses

The through-the-thickness distribution of the in-plane normal stress σ_x, for aspect ratio $l/h = 10$, is shown in Figure 8(a). The stresses are computed at the nodes with coordinates $x = y = 0$. Figures 8(b) and 8(c) contain similar plots of the interlaminar shear stresses σ_{yz} and σ_{xz}, respectively. The stresses are normalized by the relations:

$$(\bar{\sigma}_{xz}\,,\ \bar{\sigma}_{yz}) = \frac{h}{ql}(\sigma_{xz}\,,\ \sigma_{yz})\,;\quad \bar{\sigma}_x = \frac{h^2}{ql^2}\sigma_x.$$

In Figure 8(b) σ_{yz} is computed at the point $x = 0$ and $y = a$ and in Figure 8(c) σ_{xz} is computed at the point $x = a$ and $y = 0$. In these plots, broken lines represent the stresses obtained by the constitutive equations, while the smooth solid lines represent the stress distribution obtained using the equilibrium equations. The difference between the results is very clear and the excellent representation of the shear stresses demonstrated.

The same scheme, but with the sinusoidal distributed load $\left(q = q_0 \cos\dfrac{\pi x}{2a} \cos\dfrac{\pi y}{2a}\right)$ on the plate, is used to make a comparison between the shear and normal stresses calculated by the proposed element and the analogous determined using the three-dimensional exact solution of Pagano [27, 28]. The positions in which the stresses are calculated and the mesh adopted on only a quarter of the plate are the same used in the previous example. Observing the plots reported in Figures 9 we can say that the results compare very well, especially for σ_{yz} and σ_{xx}.

6.3. Ply drop-off beam problem

Ply drop-off is an important problem in the study of structures made of composite materials. A part of a layer of a composite laminate is removed in a transition from thick to thin laminates. Obtaining an exact solution or a finite element analysis of these irregular structures is a major problem. This is because the thick part has its middle surface at a different location

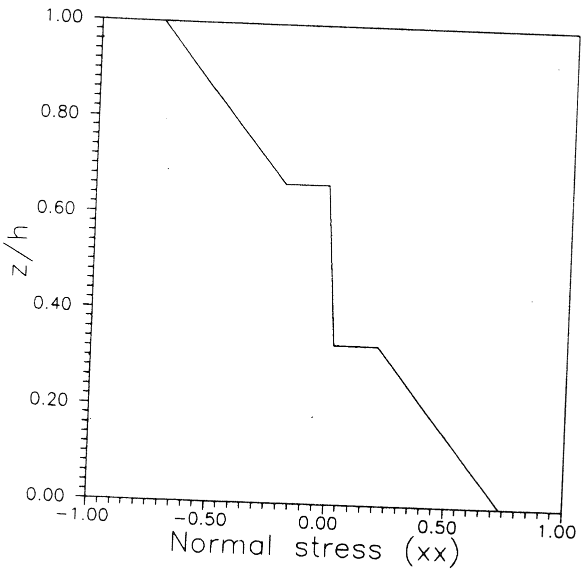

Figure 8(a). Normal stresses

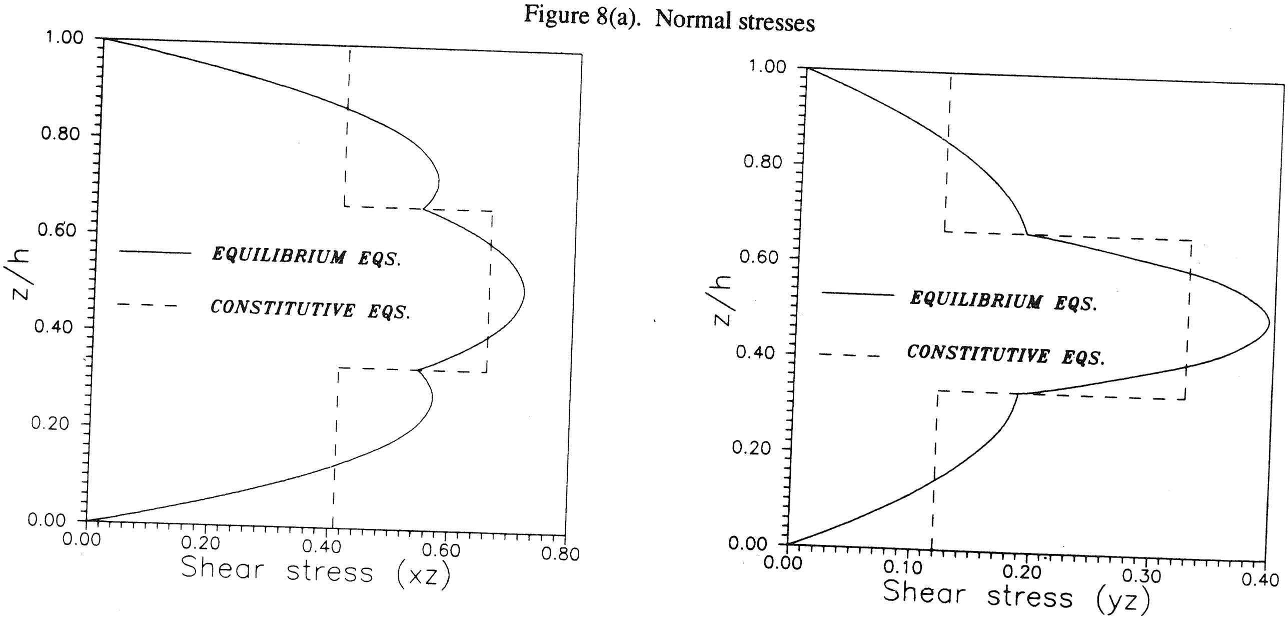

Figure 8(b) and 8(c) – Shear stresses: comparisons between equilibrium and constitutive equations

through the thickness than the thin part. By using the 3DLCS element this problem is overcome because, in comparison to the two-dimensional analysis, the position of the middle surface is not important for the use of this element.

Before considering the drop-off problem itself, the deflection obtained from 3DLCS for a cantilever beam subjected to tip load and considering the shear effect is checked. A unitary load ($P = 1.0$) was applied in the transverse direction. The deflection is calculated at two points *a* and *b* as shown in Figure 10 together with the dimensions, the labels and the boundary conditions. The material is isotropic and has the same mechanical parameters of example 6.1.1. The total deflections are calculated by adding the bending displacements w_b at the shear effects w_s (Timoshenko beam theory).

$$\text{point } A = W_t = W_b + W_s = \frac{Pl^3}{3\,EI} + \frac{Pl}{\chi\, GA} \quad (\chi = 5/6)$$

$$\text{point } B = W_t = W_b + W_s = \frac{5\,Pl^3}{48\,EI} + \frac{Pl}{2\,\chi\, GA}$$

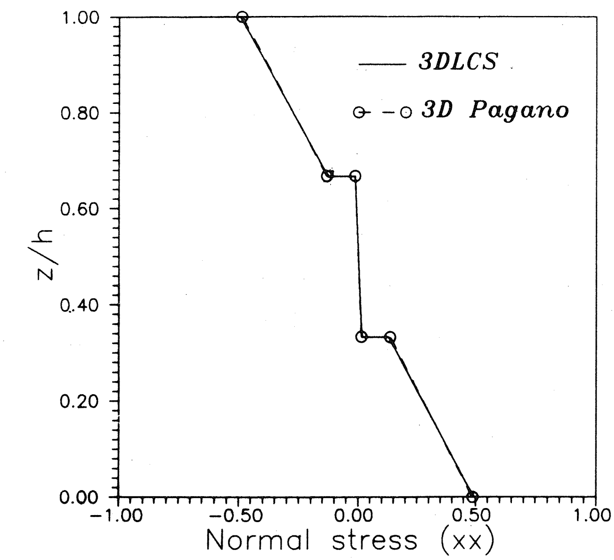

Figure 9(a). Normal stresses – Comparisons between the 3DLCS results and the tridimensional exact solution of Pagano [27, 28]

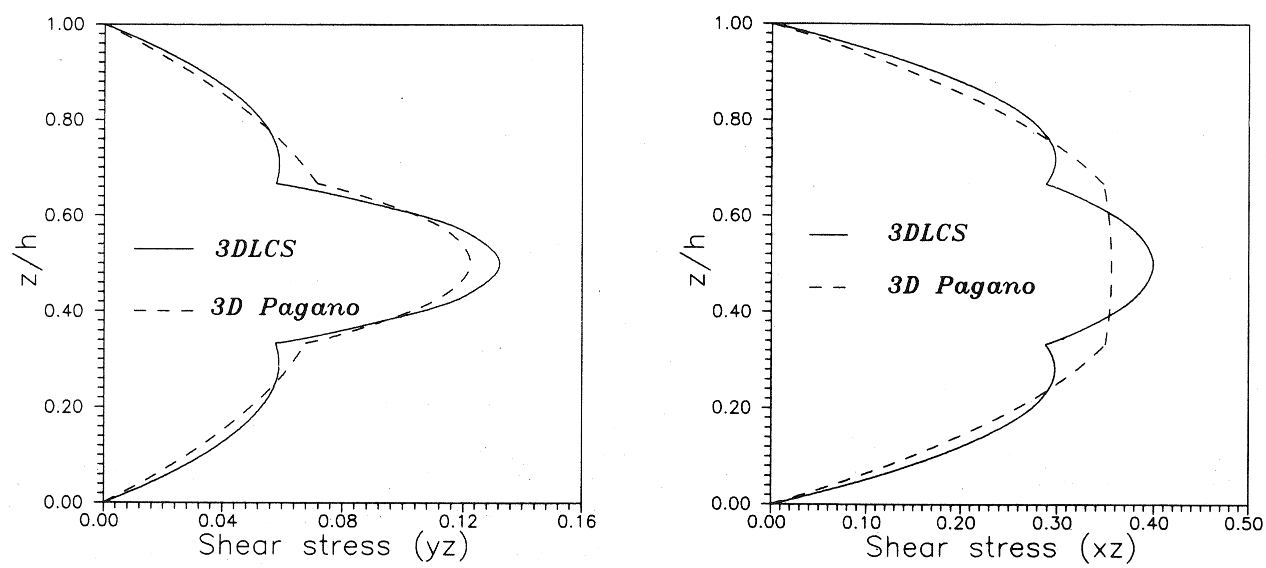

Figure 9(b) and 9(c). Shear stresses – Comparisons between the 3DLCS results and the tridimensional exact solution of Pagano [27, 28]

	l_0	W_b	W_s	W_t	W_{3DLCS}
A	5.00	0.01725	0.00053	0.01778	0.01750
B	2.50	0.00538	0.00026	0.00565	0.00552

Now the ply drop-off beam is modeled removing one element (el. num. 2) as displayed in Figure 10. In order to calculate the exact solution, the structure has to be considered in two parts. The thicker is referred to by a subscript 2 and the section with the drop-off, referred by a subscript 1.

$$W_2 = \frac{P\, l_2^3}{3\, EI_2} + \frac{P l_1\, l_2^2}{2\, EI_2} + \frac{6\, P l_2}{5\, GA_2} = W_t \,(\text{point } B)$$

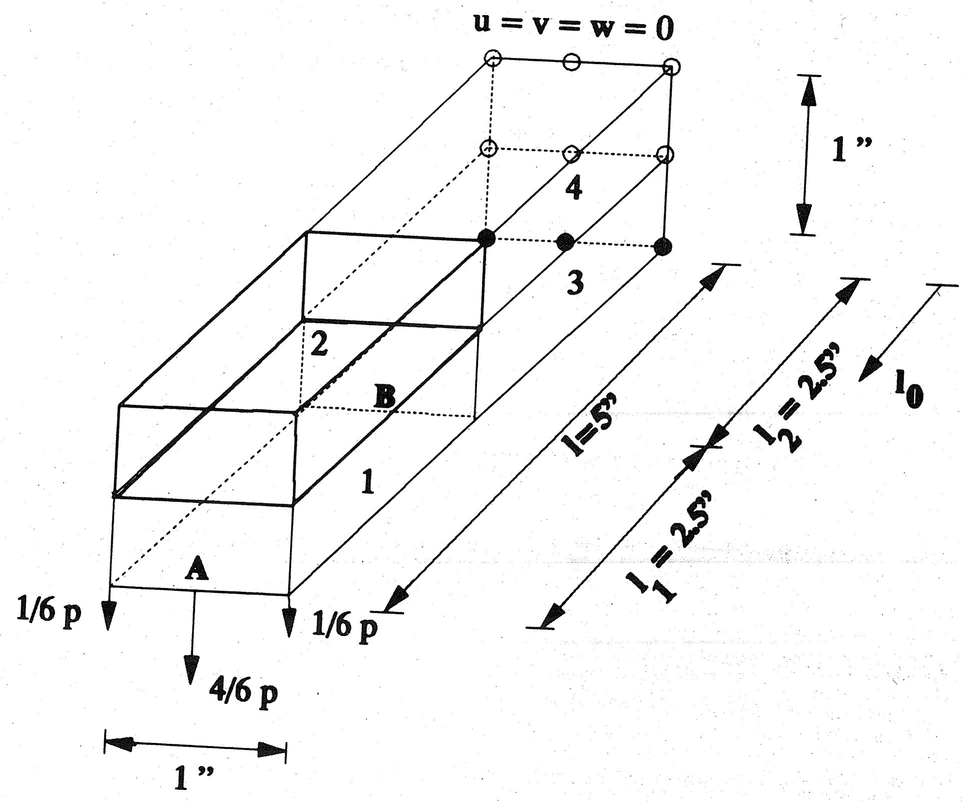

Figure 10. Ply drop-off problem

$$\theta_2 = \frac{Pl_2^2}{2\,EI_2} + \frac{Pl_1\,l_2}{EI_2}; \quad W_1 = \frac{Pl_1^3}{3\,EI_1} + \frac{6\,Pl_1}{5\,GA_1};$$

$$W_{2\,tip} = W_2 + \theta_2 \cdot l_2; \quad W_t\,(\text{point } A) = W_{2\,tip} + W_1$$

For the example depicted in Figure 10 the total transverse displacement (analytical) is equal to 0.03393″ while the Finite Element result is 0.034846″. It can be noted that the 3DLCS result is larger than the analytical solution. This is because the analytical solution assumes the two middle surfaces coincide, which is not the case in this example. It is interesting to note that at the drop-off point the normal is not straight, consequently the displacement calculated by the Finite Element model is larger than predicted analytically.

6.4. Central deflections of plates

A simply supported square plate with point load and a clamped square plate subject to uniformly transverse load are analysed to show the results making comparisons with the analogous results obtained running the commercial program NISA II [20]. The structures are made in isotropic material with the same mechanical parameters of example 6.1.1, the scheme of the structures, the boundary conditions and the loads are reported in Figure 11. The results are reported in tables 9 and 10 for two ratios of a/h.

The elements used in NISA II are described by these parameters:
NISA 3D: brick elements with 20 nodes, NKTP = 4, NORDR = 2,
NISA 2D: two dimensional thick and thin shell elements with 8 nodes, NKTP = 20, NORDR = 2.
The exact solution, obtained by using the Classical Plate Theory, is also reported [29]. It is clear that the proposed solution is the nearest solution when the structure is thin and this theory is valid. It is also very worth noting that, when the plate is thin the solution obtained using the brick elements of NISA II is very different from the other two solutions. This denotes

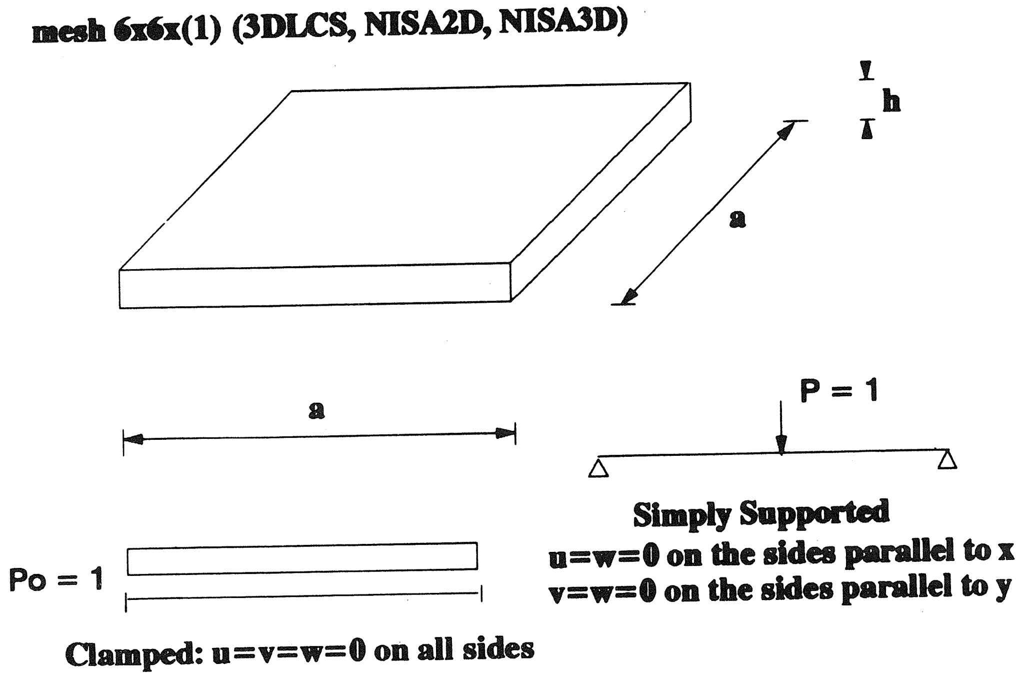

Figure 11. Isotropic plates used in the comparisons between NISA II and 3DLCS

the well known effect of the ill-conditioned equations discussed by Ahmad [17] due to the ε_z different from zero. The proposed element, instead, is a solid element but the condition that ε_z is omitted in the equations (11) and (17). Then the problem of the ill-conditioned equations is overcome. When the structure became thick the three solutions are not very different, and the proposed element shows that is the more deformable taking in better account the shear effects.

Table 9. Central deflections of simply supported isotropic plate under point load *C.P.T.* solution [29]:0.001159(Pa²)/D; D = (Eh³)/12 (1 – ν²))

a/h	*NISA3D*	*NISA2D*	*3DLCS*	*C.P.T.*
100	4.06331	4.36106	4.3919	4.38133
10	5.01545e-3	5.05799e-3	5.4028e-3	–

Table 10. Central deflections of clamped isotropic plate under uniformly distributed load *C.P.T.* solution [29]: 0.00126(P₀ a⁴)/D; D = (Eh³)/(12(1 – ν²)

a/h	*NISA3D*	*NISA2D*	*3DLCS*	*C.P.T.*
100	0.36866	0.45717	0.48006	0.47631
10	5.13700e-4	5.68437e-4	5.6896e-4	–

7. THE PRE- AND POST-PROCESSOR

The computer program has been implemented by including a subroutine to useful input the data from NISA or ABAQUS pre-processor commercial programs.

The 3DLCS model requires 18 nodes per element with 2 dof (*u* and *v*) and 9 nodes with 1 dof (*w*). The twenty nodes of NISA or ABAQUS are used to produce directly the first 16 nodes of 3DLCS with 2 dof and the first 8 nodes with 1 dof. The ninth and the eighteenth nodes of 3DLCS are produced by using the interpolation functions of the serendipity elements

(2 dimensional 8-node elements). This can be better understood by considering at Figure 12. Here we outline how to obtain the connectivities of the 3DLCS elements starting from the NISA elements. The connection with the ABAQUS elements is equivalent.

When all the structures has been discretized by running the pre-processor of NISA II (Display III) we can connect the NISA connectivities to the 3DLCS connectivities by an array, called G. The $i-th$ components of the G array has the value of the corresponding node in the NISA connectivities correlates with the $i-th$ node in the 3DLCS connectivities. Explicitly we have:

$$
\begin{array}{llll}
G(1) = 1; & G(2) = 3; & G(3) = 5; & G(4) = 7; \\
G(5) = 2; & G(6) = 4; & G(7) = 6; & G(8) = 8; \\
G(9) = 21; & G(10) = 13; & G(11) = 15; & G(12) = 17; \\
G(13) = 19; & G(14) = 14; & G(15) = 16; & G(16) = 18; \\
 & G(17) = 20; & G(18) = 22; &
\end{array}
$$

The connectivities of the NISA element which appears in the input file, is read by the element number (IEL), followed by the array $L(I)$, where I goes from 1 to 20 (note that NISA element has twenty nodes). Now the integer I is made to go from one to eight first. For each I from 1 to 8 we have

$$AN = G(I); \qquad GN = L(AN)$$

The nodal coordinates of each GN is found and, with the use of the serendipity element interpolation functions, over these first eight nodes the position of the ninth node is appropriately calculated. Although this node appears in the array of nodal coordinates, it is not part of any element at this point. So, it is very important that the coordinate of the ninth, eighteenth and twenty seventh nodes are made by using the serendipity interpolation functions, because the procedure can be used also for the shell elements. In fact, for plates it is sufficient to use the average of the coordinates. Now, this new node is labeled as $L(21)$. This process has to be repeated with I going from 10 to 17, producing a new node labeled as $L(22)$.

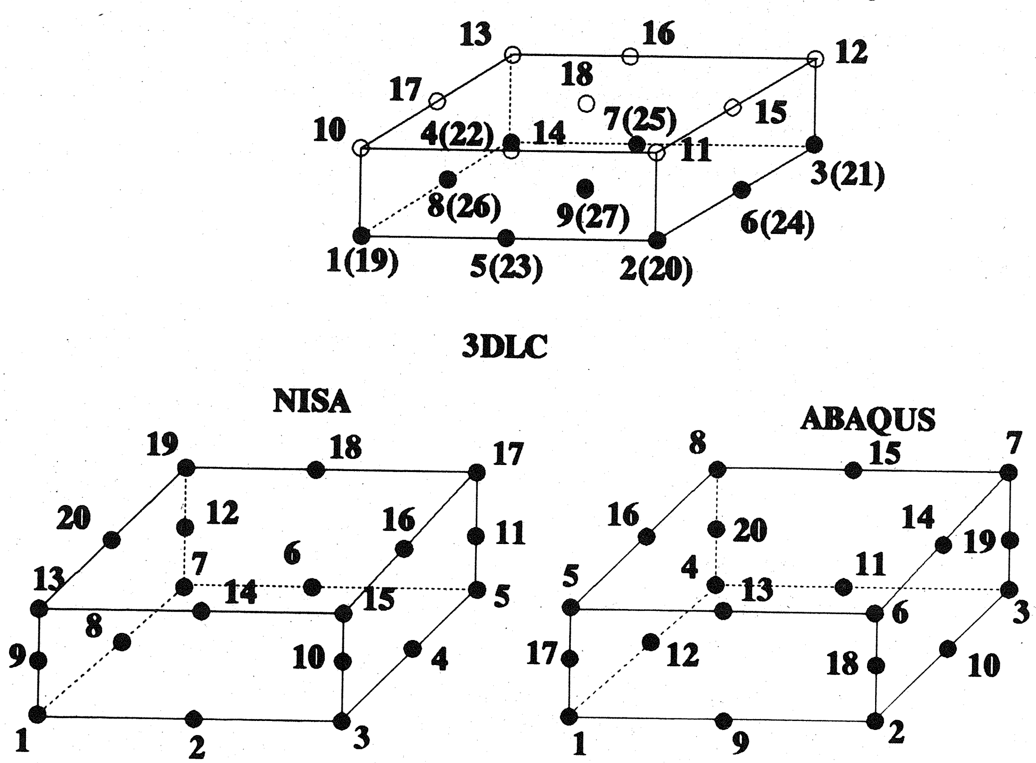

Figure 12. 3DLCS, NISA and ABAQUS elements and their connectivities

Finally we go over a loop of I from 1 to 18 and:

$$AN = G(I); \qquad C(L, I) = L(AN)$$

where C is the connectivity array of the 3DLCS elements with L being the element number and I the node. Thus for I going from 1 to 18 AN goes from 1 to 22 and the connectivities of the 3DLCS elements are written completely.

Forces and boundary conditions are read directly from the NISA input file.

To use of the post-processor of NISA is only needed to extrapolate the results (the stresses for example) from the Gauss points to the nodal points or in the centre of each element, as described by Cook [22]. Then it is only necessary to write the opportune files with the formats prescribed by the NISA post-processor (DISP-POST).

8. CONCLUSIONS

Some notes are relevant on this new elements; in particular the linear variation through the thickness of the element presents several advantages as follows:

(a) it reproduces the FSDT kinematic assumption when a single element is used to model the entire thickness of the laminate. The numerical integration must be performed layer by layer;
(b) it reproduces the LCS Theory kinematic constraints when the element is used to model a single layer of laminate. It was demonstrated (Barbero [7]) by comparison with exact solutions that the layer-wise linear distribution is the most efficient one. Therefore, more refined approximations through the thickness (e.g. quadratic, cubic spline) are usually not necessary. However, they can be easily implemented;
(c) the computational cost is reduced with respect to three-dimensional quadratic finite elements (20 or 27 node brick elements).

Appendix I. List of Symbols

x, y, z	Global coordinates
1, 2, 3	Lamina natural directions (1 = fibre direction)
ξ, η, ζ	Elemental coordinates
N_i	Interpolations functions in global coordinates
$\overline{N}_i$	Interpolation functions for the global coordinate definitions
$\{\mathbf{u}\} = \{u, v, w\}^T$	Displacement vector
$\{\boldsymbol{\delta}_\mathbf{i}\} = \{u_i, v_i, w_i\}^T$	Nodal displacement vector
$\{\boldsymbol{\delta}^\mathbf{e}\}$	Elemental displacement vector
n, n_e	Number of nodes in the mesh and in the element, respectively
$\{\sigma\}$; $\{\sigma'\}$	Stress vectors in global and local coordinates, respectively
$\{\varepsilon\}$; $\{\varepsilon'\}$	Strain vectors in global and local coordinates, respectively
$[C_{ij}]$	Three dimensional stiffness matrix
$[Q_{ij}]$	Two dimensional stiffness matrix
$[D_{ij}]$	3DLCS stiffness matrix
K	Shear correction factor
E_1, E_2, E_3	Young's moduli in direction 1, 2, and 3, respectively
G_{12}, G_{13}, G_{23}	Shear moduli
$\nu_{12}, \nu_{13}, \nu_{23}$	Poisson coefficients
$[\mathbf{T}^k]$	rotation matrix for the generic lamina k
Π	Total potential energy
$\{\mathbf{F_p}\}$	Equivalent nodal forces due to applied pressure
$\{\mathbf{p}\} = \{p_x, p_y, p_z\}^T$	Body forces per unit volume

$\{\mathbf{q}\}$	Applied surface tractions
$[\mathbf{B}]$	Strain matrix in global coordinates
$[\mathbf{K}]$	Plate stiffness matrix in global coordinates
$\{\mathbf{F}\}$	Equivalent nodal forces
$[\mathbf{J}]$	Jacobian matrix
$[\mathbf{B}_x]$, $[\mathbf{B}_y]$	Matrices of second derivatives of interpolation functions with respect to x and y co-ordinate, respectively
P_i	Component of the distributed load in direction i
A	Area of upper, middle or bottom surface of the 3DLCS element, depending on the position of the loading
TH	Thickness of the 3DLCS element at each Gaussian point
W	Weight at each Gaussian point
ngp	number of Gaussian points

Appendix II. Computation of higher-order derivatives

The computation of the second derivatives of the interpolation functions with respect to the global coordinates involves additional computations.

The first order derivatives with respect to the global coordinates are related to those with respect to the elemental coordinate according to:

$$\begin{Bmatrix} \dfrac{\partial N_i}{\partial x} \\ \dfrac{\partial N_i}{\partial y} \\ \dfrac{\partial N_i}{\partial z} \end{Bmatrix} = \begin{bmatrix} \dfrac{\partial x}{\partial \xi} & \dfrac{\partial y}{\partial \xi} & \dfrac{\partial z}{\partial \xi} \\ \dfrac{\partial x}{\partial \eta} & \dfrac{\partial y}{\partial \eta} & \dfrac{\partial z}{\partial \eta} \\ \dfrac{\partial x}{\partial \zeta} & \dfrac{\partial y}{\partial \zeta} & \dfrac{\partial z}{\partial \zeta} \end{bmatrix}^{-1} \begin{Bmatrix} \dfrac{\partial N_i}{\partial \xi} \\ \dfrac{\partial N_i}{\partial \eta} \\ \dfrac{\partial N_i}{\partial \zeta} \end{Bmatrix} = [\mathbf{J}]^{-1} \begin{Bmatrix} \dfrac{\partial N_i}{\partial \xi} \\ \dfrac{\partial N_i}{\partial \eta} \\ \dfrac{\partial N_i}{\partial \zeta} \end{Bmatrix} \tag{AII-1}$$

where the Jacobian $[\mathbf{J}]$ is evaluated using the approximation of the geometry (1).

The second derivative of N_i with respect to the elemental coordinate (x, y, z) are given by:

$$\begin{Bmatrix} \dfrac{\partial^2 N_i}{\partial \xi^2} \\ \dfrac{\partial^2 N_i}{\partial \eta^2} \\ \dfrac{\partial^2 N_i}{\partial \zeta^2} \\ \dfrac{\partial^2 N_i}{\partial \eta\, \partial \zeta} \\ \dfrac{\partial^2 N_i}{\partial \xi\, \partial \zeta} \\ \dfrac{\partial^2 N_i}{\partial \xi\, \partial \eta} \end{Bmatrix} = [\mathbf{J^1}] \begin{Bmatrix} \dfrac{\partial^2 N_i}{\partial x^2} \\ \dfrac{\partial^2 N_i}{\partial y^2} \\ \dfrac{\partial^2 N_i}{\partial z^2} \\ \dfrac{\partial^2 N_i}{\partial y\, \partial z} \\ \dfrac{\partial^2 N_i}{\partial x\, \partial z} \\ \dfrac{\partial^2 N_i}{\partial x\, \partial y} \end{Bmatrix} + [\mathbf{J^2}] \begin{Bmatrix} \dfrac{\partial N_i}{\partial x} \\ \dfrac{\partial N_i}{\partial y} \\ \dfrac{\partial N_i}{\partial z} \end{Bmatrix} \tag{AII – 2}$$

Then the second derivative respect to the global coordinate are given by:

$$\left\{\begin{matrix} \dfrac{\partial^2 N_i}{\partial x^2} \\ \dfrac{\partial^2 N_i}{\partial y^2} \\ \dfrac{\partial^2 N_i}{\partial z^2} \\ \dfrac{\partial^2 N_i}{\partial y \partial z} \\ \dfrac{\partial^2 N_i}{\partial x\, \partial z} \\ \dfrac{\partial^2 N_i}{\partial x\, \partial y} \end{matrix}\right\} = [\,\mathbf{J^1}\,]^{-1} \left(\left\{\begin{matrix} \dfrac{\partial^2 N_i}{\partial \xi^2} \\ \dfrac{\partial^2 N_i}{\partial \eta^2} \\ \dfrac{\partial^2 N_i}{\partial \zeta^2} \\ \dfrac{\partial^2 N_i}{\partial \eta\, \partial \zeta} \\ \dfrac{\partial^2 N_i}{\partial \xi\, \partial \zeta} \\ \dfrac{\partial^2 N_i}{\partial \xi\, \partial \eta} \end{matrix}\right\} - [\,\mathbf{J^2}\,] \left\{\begin{matrix} \dfrac{\partial N_i}{\partial x} \\ \dfrac{\partial N_i}{\partial y} \\ \dfrac{\partial N_i}{\partial z} \end{matrix}\right\} \right) \qquad \text{(AII – 3)}$$

where the coefficients of $[\,\mathbf{J^1}\,]$ and $[\,\mathbf{J^2}\,]$ are the following:

$$J^1_{11} = \left(\frac{\partial x}{\partial \xi}\right)^2; \qquad J^1_{12} = \left(\frac{\partial y}{\partial \xi}\right)^2; \qquad J^1_{13} = \left(\frac{\partial z}{\partial \xi}\right)^2;$$

$$J^1_{14} = 2\frac{\partial y}{\partial \xi}\frac{\partial z}{\partial \xi}; \qquad J^1_{15} = 2\frac{\partial x}{\partial \xi}\frac{\partial z}{\partial \xi}; \qquad J^1_{16} = 2\frac{\partial x}{\partial \xi}\frac{\partial y}{\partial \xi};$$

$$J^1_{21} = \left(\frac{\partial x}{\partial \eta}\right)^2; \qquad J^1_{22} = \left(\frac{\partial y}{\partial \eta}\right)^2; \qquad J^1_{23} = \left(\frac{\partial z}{\partial \eta}\right)^2;$$

$$J^1_{24} = 2\frac{\partial y}{\partial \eta}\frac{\partial z}{\partial \eta}; \qquad J^1_{25} = 2\frac{\partial x}{\partial \eta}\frac{\partial z}{\partial \eta}; \qquad J^1_{26} = 2\frac{\partial x}{\partial \eta}\frac{\partial y}{\partial \eta};$$

$$J^1_{31} = \left(\frac{\partial x}{\partial \zeta}\right)^2; \qquad J^1_{32} = \left(\frac{\partial y}{\partial \zeta}\right)^2; \qquad J^1_{33} = \left(\frac{\partial z}{\partial \zeta}\right)^2;$$

$$J^1_{34} = \frac{\partial y}{\partial \zeta}\frac{\partial z}{\partial \zeta}; \qquad J^1_{35} = \frac{\partial x}{\partial \zeta}\frac{\partial z}{\partial \zeta}; \qquad J^1_{36} = \frac{\partial x}{\partial \zeta}\frac{\partial y}{\partial \zeta};$$

$$J^1_{41} = \frac{\partial x}{\partial \eta}\frac{\partial x}{\partial \zeta}; \qquad J^1_{42} = \frac{\partial y}{\partial \eta}\frac{\partial y}{\partial \zeta}; \qquad J^1_{43} = \frac{\partial z}{\partial \eta}\frac{\partial z}{\partial \zeta};$$

$$J^1_{44} = 2\frac{\partial y}{\partial \eta}\frac{\partial z}{\partial \zeta} + \frac{\partial z}{\partial \eta}\frac{\partial y}{\partial \zeta}; \quad J^1_{45} = 2\frac{\partial x}{\partial \eta}\frac{\partial z}{\partial \zeta} + \frac{\partial x}{\partial \zeta}\frac{\partial z}{\partial \eta}; \quad J^1_{46} = 2\frac{\partial x}{\partial \eta}\frac{\partial y}{\partial \zeta} + \frac{\partial y}{\partial \eta}\frac{\partial x}{\partial \zeta};$$

$$J^1_{51} = \frac{\partial x}{\partial \xi}\frac{\partial x}{\partial \zeta}; \qquad J^1_{52} = \frac{\partial y}{\partial \xi}\frac{\partial y}{\partial \zeta}; \qquad J^1_{53} = \frac{\partial z}{\partial \xi}\frac{\partial z}{\partial \zeta};$$

$$J^1_{54} = \frac{\partial y}{\partial \xi}\frac{\partial z}{\partial \zeta} + \frac{\partial y}{\partial \zeta}\frac{\partial z}{\partial \xi}; \quad J^1_{55} = \frac{\partial x}{\partial \xi}\frac{\partial z}{\partial \zeta} + \frac{\partial x}{\partial \zeta}\frac{\partial z}{\partial \xi}; \quad J^1_{56} = \frac{\partial x}{\partial \xi}\frac{\partial y}{\partial \zeta} + \frac{\partial x}{\partial \zeta}\frac{\partial y}{\partial \xi};$$

$$J^1_{61} = \frac{\partial x}{\partial \xi}\frac{\partial x}{\partial \eta}; \qquad J^1_{62} = \frac{\partial y}{\partial \xi}\frac{\partial y}{\partial \eta}; \qquad J^1_{63} = \frac{\partial z}{\partial \xi}\frac{\partial z}{\partial \eta};$$

$$J^1_{64} = \frac{\partial y}{\partial \xi}\frac{\partial z}{\partial \eta} + \frac{\partial y}{\partial \eta}\frac{\partial z}{\partial \xi}; \quad J^1_{65} = \frac{\partial x}{\partial \xi}\frac{\partial z}{\partial \eta} + \frac{\partial x}{\partial \eta}\frac{\partial z}{\partial \xi}; \quad J^1_{66} = \frac{\partial x}{\partial \xi}\frac{\partial y}{\partial \eta} + \frac{\partial x}{\partial \eta}\frac{\partial y}{\partial \xi};$$

$$J^2_{11} = \frac{\partial^2 x}{\partial \xi^2}; \qquad J^2_{12} = \frac{\partial^2 y}{\partial \xi^2}; \qquad J^2_{13} = \frac{\partial^2 z}{\partial \xi^2};$$

$$J^2_{21} = \frac{\partial^2 x}{\partial \eta^2}; \qquad J^2_{22} = \frac{\partial^2 y}{\partial \eta^2}; \qquad J^2_{23} = \frac{\partial^2 z}{\partial \eta^2};$$

$$J^2_{31} = \frac{\partial^2 x}{\partial \zeta^2}; \qquad J^2_{32} = \frac{\partial^2 y}{\partial \zeta^2}; \qquad J^2_{33} = \frac{\partial^2 z}{\partial \zeta^2};$$

$$J^2_{41} = \frac{\partial^2 x}{\partial \eta \, \partial \zeta}; \qquad J^2_{42} = \frac{\partial^2 y}{\partial \eta \, \partial \zeta}; \qquad J^2_{43} = \frac{\partial^2 z}{\partial \eta \, \partial \zeta};$$

$$J^2_{51} = \frac{\partial^2 x}{\partial \xi \, \partial \zeta}; \qquad J^2_{52} = \frac{\partial^2 y}{\partial \xi \, \partial \zeta}; \qquad J^2_{53} = \frac{\partial^2 z}{\partial \xi \, \partial \zeta};$$

$$J^2_{61} = \frac{\partial^2 x}{\partial \xi \, \partial \eta}; \qquad J^2_{62} = \frac{\partial^2 y}{\partial \xi \, \partial \eta}; \qquad J^2_{63} = \frac{\partial^2 z}{\partial \xi \, \partial \eta};$$

ACKNOWLEDGEMENTS

The first author acknowledges partial support by NATO Grant CRG 910943.

The second author would like to express sincere gratitude to his advisors, Proff. Domenico Bruno and Giuseppe Spadea, for the encouragement to develop the work presented here, and gratefully acknowledges the financial support of the Italian Ministry of University (Ph. D. courses).

REFERENCES

1. E. Reissner, *The effect of transverse shear deformation on the bending of elastic plates* - J. Appl. Mech., 12, A69 (1945)
2. E. Reissner, *Small bending and stretching of sandwich type shells* - NACA-TN-1832, (1949)
3. R.D. Mindlin, *Influence of rotatoria inertia and shear on flexural motions of isotropic elastic plates* - J. Appl. Mech., 18, 31 (1951)
4. J.N. Reddy, *Exact solutions of moderately thick laminated shells* - J. Engng. Mech. Div., ASCE 110, 794 (1984)
5. J.N. Reddy, *A generalization of two dimensional theories of laminated plates* - Commun. Appl. Numer. Meth., 3, 113-180 (1987)
6. J.N. Reddy, *On the generalization of displacement-based laminate theories* - App. Mech. Rev., 42(11), S213-S222 (1989)
7. E.J. Barbero, *On a generalized laminate plate theory with application to bending, vibration and delamination buckling in composite laminates* - Ph. D. Dissertation, Virginia Polytechnic Institute and State University, Blacksburg, VA (1989)
8. E.J. Barbero, J.N. Reddy and J.L. Teply. *General two-dimensional theory of laminated cylindrical shells* - AIAA J., 28(3), 544-553 (1990)
9. S. Srinivas, *Refined analysis of composite laminates* - J. Sound. And Vibr., 30, 495-507 (1973)
10. P. Seide, *An improved approximate theory for the bending of laminated plates* - Mechanics Today, 5, 451-466 (1980)
11. M. Epstein and P.G. Glockner, *Non linear analysis of multilayered shells* - Int. J. Solids Struct., 13, 1081-1089 (1977)
12. M. Epstein and H.P. Huttelmajer, *A finite element formulation for multilayered and thick plates* - Computer & Struct., 16, 645-650 (1983)
13. H. Murakami, *Laminated composite plate theories with improved inplane responses* - ASME Pressure Vessels and Piping Conference, 257-263 (1984)
14. R. L. Hinrichsen and A.N. Palazzotto, *The Nonlinear finite element analysis of thick composite plates using a cubic spline function* - AIAA J., 24, 1836-1842 (1986)
15. D.R.J. Owen and Z.H. Li, *A refined analysis of laminated plates by finite element displacement methods - I Fundamentals and static analysis; II Vibrations and stability - Comp. & Struct., 26, 907-923 (1987)*
16. E.J. Barbero, *A 3-D finite element for laminated composites with a 2-D kinematic constraints* - Comp. & Struct., 45(2), 263-271 (1992)
17. S. Ahmad, B. M. Irons and O. C. Zienkiewicz, *Analysis of thick and thin shell structures by curved finite elements* - Int. J. Num. Meth. Engng., 2, 419-451 (1970)
18. R.A. Chaudhuri, *An equilibrium method for the prediction of transverse shear stresses in a thick laminated plate* - Comp. & Struct., 23, 139-146 (1986)
19. E.J. Barbero and J.N. Reddy, *An accurate determination of stresses in thick laminates using a generalized plate theory* - Int. J. Num. Meth. Engng. 29, 1-14, (1990)

20. NISA II Version 90.0 and DISPLAY III - Pre- and Post-Processing program Version 91.0; User's Manuals Engng. Mech. Res. Corp. (1990-1991)
21. R. M. Jones, *Mechanics of composite materials*- Hemisphere Publishing Corp., New York (1975)
22. R.D. Cook, *Concepts and applications of finite element analysis* - 2nd Ed. John Wiley, New York (1974)
23. J.N. Reddy, E.J. Barbero and J.L. Teply, *A plate bending element based on a generalized laminate plate theory* - Int. J. Num. Meth. Engng., 28, 2275-2292 (1989)
24. R.C. Averil, *On the nonlinear behaviour of shear deformable plate elements* - Thesis, Virginia Polithecnic Institute and State University, Blacksburg, VA (1989)
25. R.L. Taylor, J.C. Simo, O.C. Zienkiewicz and A.C.H. Chan, *The patch test - a condition for assessing FEM convergence* - Int. J. Num. Meth. Engng., 22, 39-62 (1986)
26. A. Razzaque, *The patch test for elements* - Int. J. Num. Meth. Engng., 22, 63-71 (1986)
27. N.J. Pagano, *Exact solutions for composite laminates in cylindrical bending* - J. Comp. Mat., 3, 398-411 (1969)
28. N. J. Pagano, *Exact solutions for rectangular bidirectional composites and sandwich plates* - J. Comp. Mat., 4, 20-35 (1970)
29. A. C. Ugural, *Stresses in plates and shells* - McGraw-Hill Book Company, New York (1981)